

Chapter 4. Semiconductor Lasers: Physics and Applications

Academic and Research Staff

Professor Rajeev J. Ram, Dr. Jianyao Chen

Visiting Scientists and Research Affiliates

Dieter Graef

Graduate Students

Ravindra V. Dalal, Steven G. Patterson, Farhan Rana

4.1 Introduction

We are developing novel semiconductor lasers to improve the performance of communications systems. Our approach is to build an understanding of these devices that is solidly rooted in electromagnetic modeling, quantum mechanics and condensed matter physics. In the past, we have developed devices that exploit physical phenomena such as (1) Bose-Einstein condensation and coherent population transients, (2) novel fabrication processes such as wafer fusion and x-ray lithography, and (3) novel device designs such as surface-emitting microcavities and quantum cascade lasers to improve devices.

In the last year, several significant advances have been made. These include,

- the development of efficient numerical algorithms for energy band structure calculations
- the development of x-ray diffraction for characterizing the interfaces between optical thin films such as distributed Bragg reflectors
- the prediction and demonstration of low distortion signal transmission achieved by cancellation of spatial-hole burning and gain compression nonlinearities in DFB lasers, and
- the construction of an analog fiber link utilizing ultracompact surface emitting laser sources.

These are among the results discussed in the following sections. Extensive discussion will be presented in several forthcoming journal publications.

4.2 Band Structure and Optical Gain in Strained Layer Quantum Wells

Sponsor

MIT Lincoln Laboratory
Contract BX-6558

Project Staff

Farhan Rana, Professor Rajeev J. Ram

Design of high-performance semiconductor lasers requires a careful and detailed consideration of the physical processes involved. In the case of lasers operating at high modulation frequencies and high output power levels, non-equilibrium effects associated with carrier transport, carrier relaxation in quantum wells and carrier heating effects are important. Analytical models currently available to describe laser physics have little accuracy. Design of novel high-performance lasers require efficient and powerful computer simulation tools. Unlike passive devices, active optical devices have a rich variety of physics ranging from the microscopic to the macroscopic level. In order to design semiconductor lasers one needs to know the band structure of strained quantum wells, laser gain, radiative and Auger recombination rates, carrier leakage rates, non-equilibrium carrier dynamics. Careful design of optical waveguiding structures and gratings (in the case of DFB lasers) is also crucial. In addition, microwave propagation characteristics of metal contacts are also of importance especially at high frequencies. We have developed a suite of modeling tools for the accurate simulation of various laser structures:

1. **Band Structure Solver:** We have implemented an efficient finite difference technique to solve band structure of strained quantum wells using an eight-band $k \cdot p$ approach. This scheme also gives us the k -dependent wavefunctions

for the conduction and the valence band states. An efficient algorithm is developed by a novel implementation of the axial approximation which accurately treats the conduction and split-off valence bands. Figure 1 shows the calculated valence band structure in the quantum well active region.

2. **Carrier Dynamics and Gain:** Using results from (1) above, this program calculates laser gain, radiative recombination rates, many body effects related to carrier density dependent bandgap renormalization and index change. A sample gain spectrum is shown in figure 2. Non-equilibrium effects are simulated by solving a system of coupled differential equations that describe carrier scattering from acoustic phonons, optical phonons and with other carriers, and carrier recombination via stimulated and spontaneous emission of photons and via Auger processes. The solution of these equations give the non-equilibrium hot carrier distribution in k-space. Our model currently treats carrier-carrier scattering only phenomenologically and cannot simulate carrier transport in cladding layers. Future work is planned to remedy these shortcomings.
3. **Auger Recombination Rates:** The Auger solver calculates Auger recombination rates in quantum wells using the actual band structure and wavefunctions found by (1) above and the non-equilibrium carrier distribution found in (2) above. This will be the first accurate estimate of Auger recombination rates; Auger is the dominant nonradiative recombination process in lasers used for long-distances communications.
4. **Inter-Valence Band Absorption Rates:** Optical loss in semiconductor lasers caused by inter-valence band absorption in p-doped layers can reach as high as 40 cm^{-1} for 10^{18} cm^{-3} doping level. Using results from (1) and (2) this program calculates these optical losses from first principles.
5. **Optical Mode Solver:** We have implemented a 2D finite element scheme to calculate optical modes in semiconductor laser waveguides. The mode solver can find modes for the scalar wave equation and also for the semi-vectorial wave-equation.

Models of heat flow and carrier transport will complete the tools in this development suite.

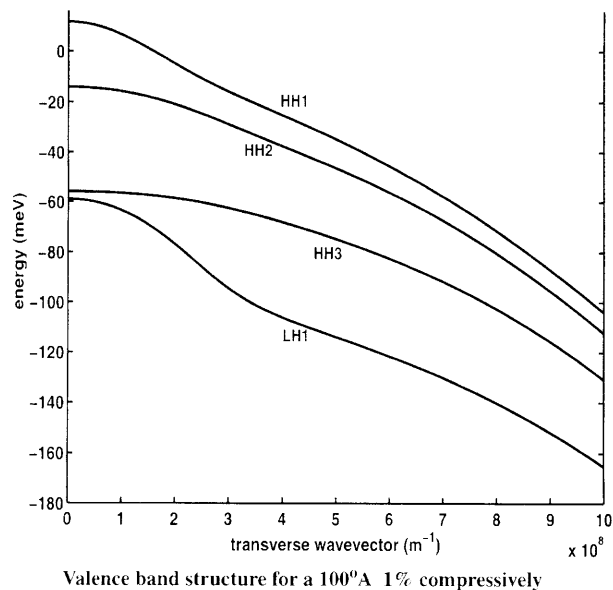


Figure 1. Valence band structure for a 100 \AA 1% compressively strained InGaAsP quantum well optimized for emission at 1.55 \mu m

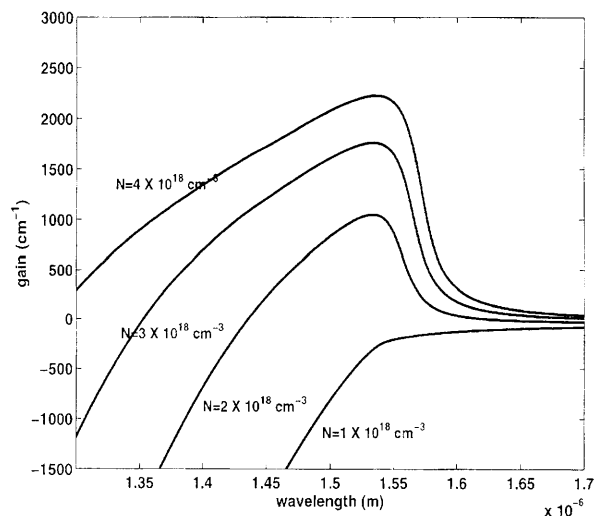


Figure 2. Gain spectrum the same quantum well as Figure 1.

4.3 Band Gap Engineering of Distributed Bragg Reflectors

Sponsor

MIT Lincoln Laboratory

Project Staff

Steven G. Patterson, Professor Leslie A. Kolodziejski, Professor Rajeev J. Ram

Vertical cavity surface emitting lasers (VCSEL) possess a number of properties which make them more attractive than conventional edge emitting laser diodes. They may be two-dimensionally packed at very high densities. It is possible to integrate them onto chips with transistor logic, drivers, and detectors. Furthermore, while edge emitting lasers typically have divergent, elliptical beams, VCSEL may be designed to have minimally divergent, circular beams, making them ideal for coupling into fibers. Finally, the end mirrors of the optical resonator do not need to be cleaved thus eliminating a costly and unreliable manufacturing step.

The physical structure of the VCSEL is similar to a p-i-n diode where the p-type and n-type regions are coincident with Distributed Bragg Reflectors (DBR). The DBR is a stack of alternating thin films of two materials with different indices of refraction, each material a quarter wavelength thick. For this work, pairs of $\text{Al}_{0.1}\text{Ga}_{0.9}\text{As}$ and $\text{Al}_{0.9}\text{Ga}_{0.1}\text{As}$ films form the DBR stack. Abrupt heterojunctions between these two materials result in large conduction barriers for holes and electrons (as large as 300 meV). Heavy uniform doping is an unacceptable solution as this greatly increases optical losses due to free carrier absorption. Hence, recent efforts have been focused on the bandgap engineering of the $\text{Al}_{0.1}\text{Ga}_{0.9}\text{As} / \text{Al}_{0.9}\text{Ga}_{0.1}\text{As}$ transition in order to reduce this barrier to current transport.

One can consider linearly grading the aluminum concentration at the junction as well as the dopant concentration. The electric field resulting from the ionized donors can be used to compensate for the heterojunction potential barrier. Figure 3 shows the conduction and valence band energies with a) only the aluminum concentration gradient and b) with both the dopant and aluminum concentration appropriately graded. A well-engineered interface does not present any barrier to carrier transport while maintaining the desired optical index change.

Achieving the appropriate control of the aluminum concentration during epitaxial growth of the DBRs requires careful characterization of the growth processes. We are able to verify that the DBR mirror has the desired composition gradients by x-ray scattering measurements. Figure 4 shows the measured and simulated x-ray diffraction spectra from a 15-period DBR. For the first time, this technique allows direct verification of the DBR alloy composition. Tools are currently being developed to study the dopant profile in these laser structures.

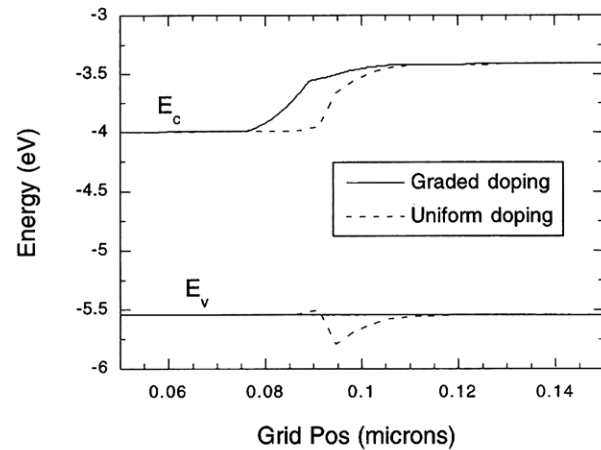


Figure 3. Calculated plots for: an $\text{Al}_{0.1}\text{Ga}_{0.9}\text{As} / \text{Al}_{0.9}\text{Ga}_{0.1}\text{As}$ heterojunction, with a 300 angstrom grading layer and modulation doping designed to flatten the valence band.

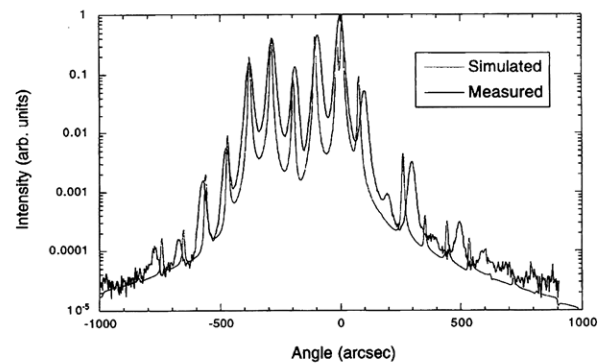


Figure 4. X-ray data and simulation for a 15-period nominally flatband DBR. The difference in location of the higher order peaks is due to a slight period drift during growth.

4.4 Thermal Oxide for Ridge-Waveguide Semiconductor Lasers

Sponsor

MIT Lincoln Laboratories
Contract BX-6558

Project Staff

Dieter Graef, Steven G. Patterson, Professor Rajeev J. Ram

The basic idea of this work is to realize an index guided GaAs-InGaAs quantum well heterostructure laser with a DFB structure to achieve single mode lasing. The lateral index guiding and the periodic index change in the propagation direction are realized by oxidation of large Al-content $\text{Al}_x\text{Ga}_{1-x}\text{As}$.

In the last few years, the technique of wet oxidation of high composition $\text{Al}_x\text{Ga}_{1-x}\text{As}$ has been developed making it possible to fabricate high performance optoelectronic devices providing current as well as optical confinement. The native oxide possesses excellent insulating properties and a low refractive index ($n \sim 1.6$). The formation of square-wall oxidation profiles was demonstrated by P.W. Evans and N. Holonyak. This technique is an exceptional method for making integrated optoelectronic devices combining the high refractive index step realized by reactive ion etching (RIE) or wet etching and the planar geometry of ion implantation. Additionally it is possible to use a single process step for both imprinting the DFB structure and providing the light and current confinement.

Several groups have previously established that the oxidation rate is exponentially dependent on the aluminum concentration (Figure 5). In the proposed device, thermal oxidation is initiated at the wafer surface and proceeds both horizontally and vertically into the semiconductor. A vertical oxide boundary can be established by linearly increasing the aluminum content with the distance into the semiconductor. Figure 5 shows the lateral profile of the ridge-waveguide as a function of oxidation time.

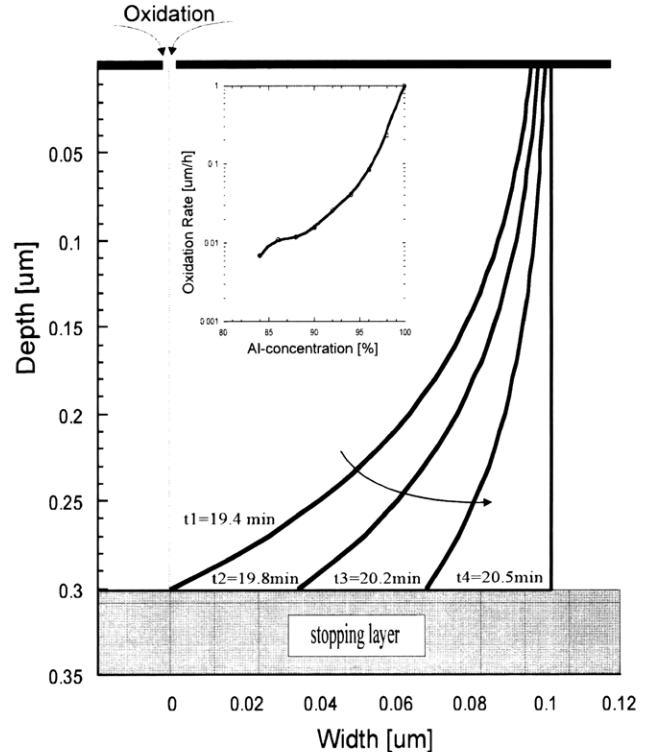


Figure 5. Lateral profile development with time for exponential rate approximation. Inset: Oxidation rate for various aluminum content.

Figure 6 uses this technique to construct an index grating along the length of the laser cavity. First a $0.5 \mu\text{m}$ GaAs (n+) buffer layer covers a (100) GaAs (n+) substrate. Then a $1.5 \mu\text{m}$ $\text{Al}_{0.95}\text{Ga}_{0.05}\text{As}$ (n) lower confining layer is grown followed by a $0.16 \mu\text{m}$ undoped GaAs waveguide with two 80 \AA $\text{In}_{0.2}\text{Ga}_{0.8}\text{As}$ QW in the center separated by a 120 \AA GaAs wall. Next an $0.3 \mu\text{m}$ upper confining layer of $\text{Al}_x\text{Ga}_{1-x}\text{As}$ (p) with a graded composition $0.88 < x < 0.95$ is grown and a 20 nm low gap $\text{Al}_x\text{Ga}_{1-x}\text{As}$ (n+) layer (stop layer for upper oxidation). The second oxidation layer (p+) is grown on the top ($0.3 \mu\text{m}$ with graded composition: $0.84 < x < 0.99$).

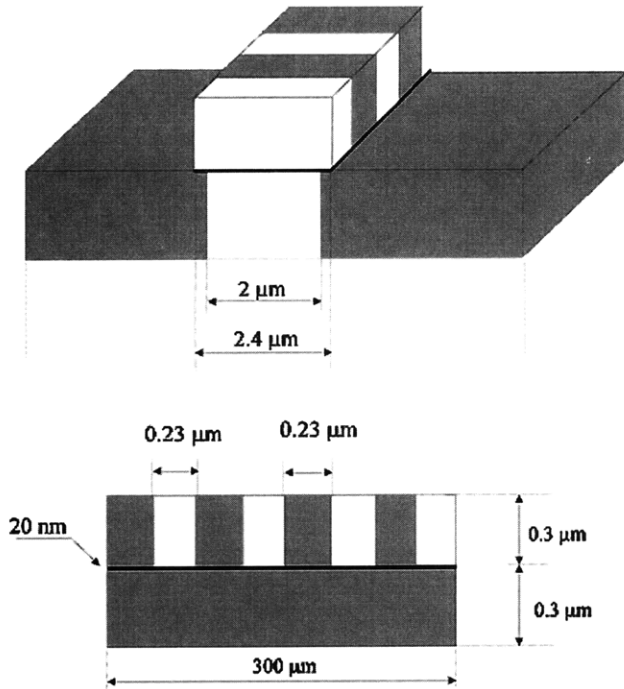


Figure 6. Basic laser structure: light and current confining oxide walls in the in the cladding layer and the DFB structure

While the buffer layer guarantees a smooth surface (on atomic scale) for the following layers the lower cladding layer is made thick enough to neglect any influence of the buffer layer on the waveguiding. The Al content of this layer is 93% to assure index symmetry in the transverse direction. The active region is formed by two InGaAs QW embedded in GaAs. The strength of the waveguide was chosen well below cut off of the second order mode to enable only the fundamental transverse mode. The upper cladding layer will be oxidized to give lateral confinement, and therefore its grading and its thickness are crucial for laser fabrication. The GaAs guiding layer acts as stopping layer for this oxidation. In order to use only one oxidation step the two graded layers can not be designed independently. They have to be grown so as to get square walls of different aspect ratios during the same oxidation step. The goal is to get a square wall periodic index change with a given duty cycle in the top layer, while making a compact confining layer in the lateral direction by oxidizing the lower graded AlGaAs layer at a higher rate. The calculated oxidation time is ~ 0.3 hours.

The laser fabrication itself begins with patterning 2.4 μm wide lines on the sample using standard lithography techniques. These stripes serve as a mask for

the fast etch of the two uppermost layers, exposing the lower AlGaAs for subsequent oxidation. The final ridge width will be 2 μm where the additional 0.4 μm account for the lateral oxidation of the lower layer. Now the protecting layer is removed and a different line pattern (0.04 μm) is deposited perpendicular to the ridge. The width of this fine line pattern is determined by the duty cycle of the DFB structure in the second order mode and the lateral oxidation rate. The sample is then immediately placed in the wet oxidation furnace (425°C; supplied with N_2 bubbled through H_2O at $\sim 95^\circ\text{C}$). When the sample is introduced in the furnace the exposed AlGaAs (both layers) start oxidizing vertically and horizontally with a rate depending on the Al-content (Figure 5). The concentration difference in the ridge will provide a square wall profile (Figure 5 and Figure 6) equal to the second order Bragg condition. At the same time the cladding layer will oxidize with a higher velocity due to its higher Al concentration resulting in twice the aspect ratio of the upper layer. Thus the material underneath the lines is also oxidized resulting in a compact insulating and light confining wall in lasing direction. Because the oxidation is isotropic in the lateral direction we get oxide (square walls) underneath a part of the ridge (Figure 6) To take account of this effect the initial ridge width was chosen larger than used for calculations.

Planar anisotropic oxidation of graded $\text{Al}_x\text{Ga}_{1-x}\text{As}$ can be used for fabricating high performance laser diodes. Once the exact Al-gradings for the two layers in question are determined, the laser structure can be formed by a single process step resulting in planar structures with high index contrast. MBE makes it possible to grow well determined grading functions. This possibility together with the strong oxidation rate dependence on the Al-content gives a very powerful tool for engineering the lateral index profile while keeping the surface planar. In addition to square walls, it is possible to produce closed loops with different curvatures, e.g., circles resulting in cylindrical wires.

4.5 High-Speed Semiconductor Laser Development

Sponsor

MIT Lincoln Laboratory
Contract BX-6558

Project Staff

Farhan Rana, Michael H. Lim, Elisabeth Marley, Professor Rajeev J. Ram, Professor Henry I. Smith, Professor Leslie A. Kolodziejski

Lasers capable of being modulated at high frequencies are a key component for high speed optical communications. Semiconductor lasers can be intensity or frequency modulated up to very high frequencies by directly varying the drive current. Direct modulation schemes are much simpler to implement than those involving external modulators. The goal of this research is to develop, design, and fabricate very high speed semiconductor lasers operating at wavelengths suitable for fiber optic communication systems.

Design requirements for high speed lasers demand that careful attention be paid to both the microscopic and the macroscopic physics of these devices. The microscopic physics includes proper design of semiconductor heterostructures. Important laser parameters such as gain, differential gain, radiative recombination rate, Auger recombination rate, frequency chirp, carrier leakage, and gain compression factor can be significantly improved by optimizing the design of semiconductor quantum wells, barriers, and cladding regions. At high modulation frequencies non-equilibrium effects such as carrier transport and relaxation in heterostructures and carrier heating also become increasingly important. At the macroscopic level, attention must be paid to the proper design of optical waveguides. For DFB (and DBR) lasers, designing optical grating structures that minimize spatial hole burning and reduce chirp, distortion and noise pose a significant challenge. The electrical characteristics of a laser including its series resistance and capacitance can also become a potential bottleneck for high speed operation. In addition, at high frequencies the distributed nature of semiconductor laser structures cannot be ignored. Laser devices must also be properly impedance matched with the electrical driving circuitry. Our research program includes looking at all the above issues for designing better and faster lasers.

We have developed techniques for fabricating polyimide-planarized ridge-waveguide laser structures that are ideally suited for high frequency operation because of their very low capacitance and low leakage currents. The low capacitance is a result of the large separation between the top metal contact and the substrate (see Figure 7). In addition, this technique allows us to make ohmic contacts to ridges without having to open contact vias lithographically. Thus, very narrow ridge structures can be realized. Crystal growth for these laser structures is also done at MIT. The grown material shows good electrical and optical characteristics.

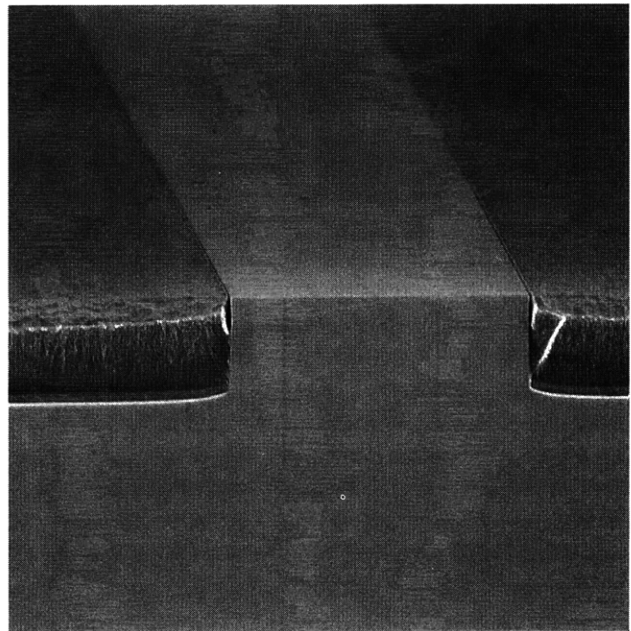


Figure 7. Scanning electron micrograph of an InP ridge waveguide with a polyimide planarization layer.

Techniques for fabricating optical gratings for DFB (and DBR) lasers using combinations of interferometric, X-ray, and spatially phase-locked e-beam lithography have also been recently developed at the Nanostructures Laboratory at MIT. These techniques allow us to make optical gratings with spatially varying feedback characteristics with long range spatial coherence which has never been done before. We plan to explore a variety of grating based semiconductor laser structures for high speed as well as for low noise operation. In addition, the high speed laser processes developed will also enable us to realize high-performance mode-locked semiconductor lasers.

4.6 Nonlinear Response of DFB Lasers

Sponsor

MIT Lincoln Laboratory
Contract BX-6558

Project Staff

Dr. Jianyao Chen, Professor Rajeev J. Ram

With the outstanding features of dynamic single frequency operation and wide modulation bandwidth, DFB lasers are the primary candidates for various analog optical fiber communication systems. For such applications, the laser light intensity is required to be a linear function of the drive current. The characteristics of nonlinearly generated harmonic and intermodulation distortions become the quantities of concern. Due to the nature of distributed feedback, various spatial features of DFB lasers, such as the asymmetric facet conditions, abrupt phase shift and nonuniform carrier injection, have strong influence on the uniformity of photon distribution inside the laser cavity. This causes the carriers in the active region to recombine at different rates at different locations. Therefore, a spatially resolved analysis of nonlinear responses in DFB lasers becomes significant.

To include the various spatial features of DFB lasers accurately and to retain the advantage of closed form analysis, the spatially dependent rate equations based on the Greens function method are developed to study the harmonic and intermodulation distortions in DFB lasers. The self-consistent analysis shows that spatial hole burning, nonlinear gain compression and relaxation oscillation are three major sources of signal distortion and that their effects can interact with each other both constructively and destructively.

Detailed frequency analysis reveals that the nonlinear distortion at low frequency depends on the uniformity of the optical field distribution significantly. The effect, however, is limited by the carrier damping rate in DFB laser. The induced distortion rolls off at range of a few hundred megahertz. Numerical results show that, as the coupling strength of DFB grating kL deviates away from the optimum value, the harmonic and intermodulation distortions can increase rapidly in the laser. On the other hand, the relaxation oscillation effect is dominated in the intermodulation distortion at high frequency, which is independent of kL . Therefore, choosing a proper grating with the optimum coupling coefficient and working away from the resonance frequency are important.

Facet reflection determines the optical field distribution in DFB laser significantly. As the grating phase at facet is cleaved randomly, the selected lasing mode can appear on either short or long wavelength sides of the Bragg stopband. Our analysis indicates that, although their optical field distributions can be similar, the induced distortions give different phases. On the other hand, gain compression and relaxation oscillation always give 0 and π phases in third order intermodulation distortion. Therefore, as we choose different grating structure and facet conditions, it is possible to make spatial hole burning effect to cancel with gain compression and relaxation oscillation effects to get very low total distortion at low and high frequencies, respectively. Such properties are very useful to the applications in high fidelity communication systems.

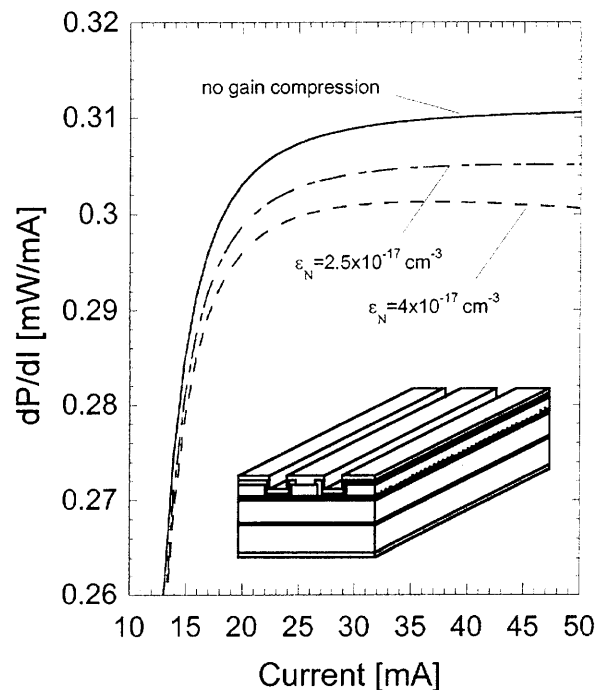


Figure 8. Slope efficiency of HR/AR coated DFB laser with grating phase $\phi = 0$ at HR facet, where inset gives the structure of ridge waveguide distributed feedback laser.

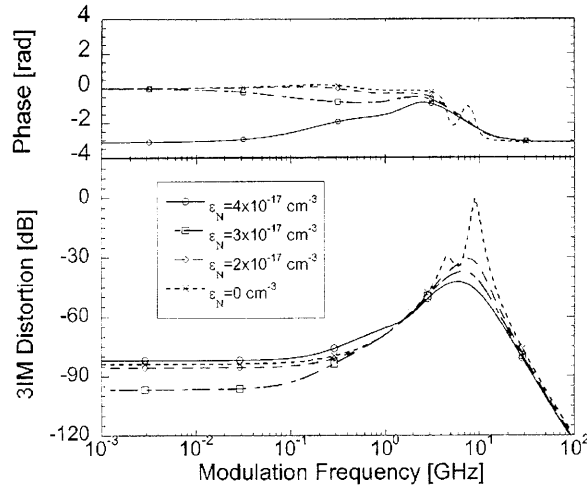


Figure 9. Frequency response of third order intermodulation distortion in of HR/AR coated DFB laser with grating phase $\phi=0$ at HR facet, where $I=I_{th}+35$ mA, $OMD=30\%$, $f_1-f_2=1$ MHz.

4.7 High-Fidelity, High-Dynamic Range Fiber Communications

Sponsor

MIT Lincoln Laboratory
Contract BX-6558

Project Staff

Ravindra V. Dalal, Dr. Jianyao Chen, Dr. Roger Helkey,¹ Harold V. Roussell,² Professor Rajeev J. Ram

Cable television providers and telecommunications companies are competing to create broad-band subscriber networks that are upgradeable, flexible, and able to carry large bandwidths of various types of data. The wide bandwidths of semiconductor lasers and the accompanying fiber optic components are cost-competitive and compatible with existing coaxial cable systems, thus making them attractive to cable providers as well as telecommunications companies. Through subcarrier multiplexing (SCM) a single network can handle multiple data formats, including voice, data, video, digital audio, high definition video, and any combination of these services. Subcarrier multiplexing has also stimulated great interest in nar-

row band analog optical applications, which include phase array radar and personal communications systems (PCS). As their name implies, these applications require a relatively narrow bandwidth of channels.

The performance of laser diodes for optical communications is limited by application bandwidth, distortion, and noise. Distortion can be caused by many factors. Static distortion occurs when the nonlinearities of the light-versus current (LI) curve are present. These nonlinearities are caused by spatial hole burning, gain compression, finite carrier transport times, and leakage currents. Dynamic distortion occurs when the nonlinearities of the device cause different frequency components to mix together through the interaction of photons and electrons in the laser cavity. As a result of these nonlinearities in the device, it is possible for frequencies from separate channels to interfere and mix with each other to produce new frequency components.

The application bandwidth determines the type of distortion that will affect the system. A narrow band system will be primarily affected by third order intermodulation distortion (IMD3). The key figure of merit for such narrow band applications is the spurious free dynamic range (SFDR), which is the range of inputs over which the output signal is unaffected by either noise or distortion.

Intermodulation distortion and dynamic range measurements were performed for a $1.3 \mu\text{m}$ packaged Fujitsu DFB laser (model FLD130F3ACH-AL), which is made for CATV signal distribution. The laser is designed to minimize second order intermodulation distortion. A standard two-tone electrical modulation (Figure 10) is used to study the nonlinear response of the laser.

¹ MIT Lincoln Laboratories, Lexington, Massachusetts.

² Center for Compound Semiconductor Technology, Sandia National Laboratory, Albuquerque, New Mexico.

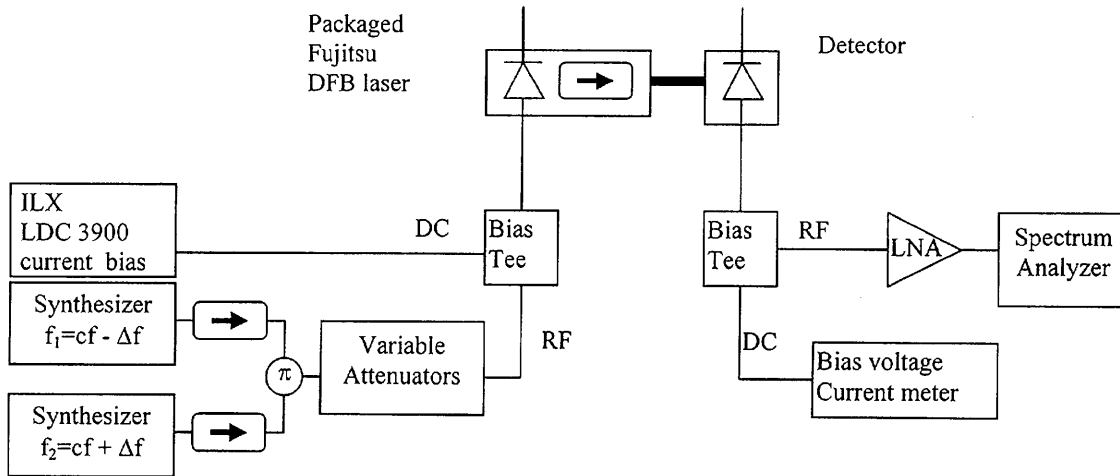


Figure 10. Experimental set-up for two-tone modulation test of an optical communications link.

We found that the SFDR peaks because of a minimum in the third order intermodulation distortion rather than because of a minimum in the noise, as can be seen in Figure 11. We believe that the distortion minimum occurs due to a cancellation in spatial hole burning and gain compression, two nonlinear effects which are dependent on the photon density in opposite ways for this particular structure for particular operating conditions. This suggests that an improved laser design may be realized by adjusting the spatial hole burning and gain compression such that the distortion minimum coincides with the minimum in the noise, thus leading to a larger SFDR. It has been shown that improving the SFDR by as little as 4 dB $\text{Hz}^{2/3}$ can double the maximum number of channels that a cellular telephone system can handle while ensuring a certain call blocking probability. A maximum SFDR of 125.5 dB $\text{Hz}^{2/3}$ was measured for the Fujitsu device, which is significantly greater than the dynamic range required for PCS (72-83 dB $\text{Hz}^{2/3}$).

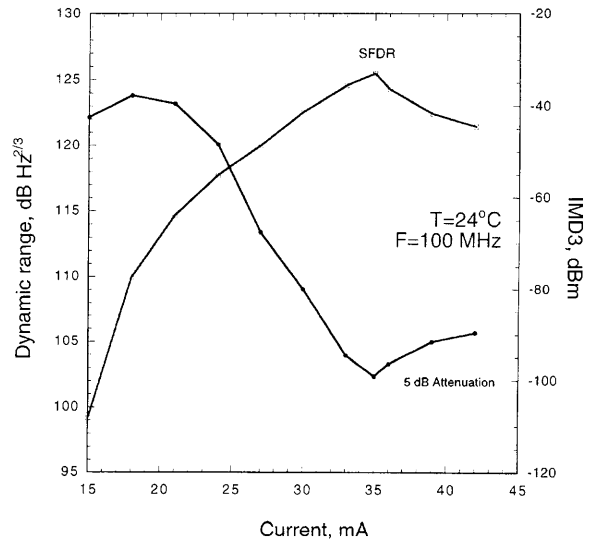


Figure 11. Spurious intermodulation free dynamic range and noise figure versus bias current for a system employing a high-linearity DFB laser.

4.8 Device Level Modeling of Communication Systems

Sponsor

MIT Lincoln Laboratory
Contract BX-6558

Project Staff

Dr. Jianyao Chen, Ravindra V. Dalal, Professor Rajeev, J. Ram, Dr. Roger Helkey

Due to the nature of distributed feedback, various spatial features in DFB lasers have great influence on device characteristics and hence determines the performance for the fiber optic system significantly. To achieve the optimum design for adequate signal quality, a detailed investigation of the influence of various structures of DFB lasers to the system performance of analog fiber optic links is therefore important. We present the first such simulation and reveal that cancellations between different nonlinearities are significant enough to suppress the signal distortions in the system.

In general, link gain, noise figure and intermodulation distortion free dynamic range are the most important quantities to concern for the high fidelity, narrow band SCM fiber optic systems. Since nonuniform photon distribution in DFB lasers gives a complex influence to the laser power output, noise performance and linearity of laser response under direct modulation, we extensively study the dependence of those parameters on various structure details of DFB grating, such as complex grating, facet coating, abrupt phase shift and etc. The revealed knowledge is very helpful to the optimization of system performance.

A strong grating feedback confines the optical field inside the DFB laser and hence reduces the laser's external quantum efficiency, which directly leads to decrease link gain for signal transmission in the system. On the other hand, weaker grating feedback makes the laser have a higher threshold which increases the intensity noise level in the laser output and hence lowers the signal-noise-ratio of the system. Theoretical study helps understand that the cancellation between spatial hole burning and gain compression effects is very useful to achieve a very high IM free dynamic range in DFB lasers.

4.9 Analog Signal Transmission Using Surface Emitting Lasers

Sponsor

U.S. Navy – Office of Naval Research/MURI

Project Staff

Ravindra V. Dalal, Dr. Roger Helkey, Harold V. Russell, Dr. Kent D. Choquette, Professor Rajeev J. Ram

Vertical cavity surface emitting lasers (VCSEL) have potential to be low cost sources for optical communications. For digital applications, transmission rates of up to 10 Gb/s for short wavelength lasers have been demonstrated, and 2.5 Gb/s at long wavelength lasers. However, the performance of VCSEL under analog modulation has not been investigated. These applications require a large carrier to noise ratio, high bandwidths, low intermodulation distortion, and wide dynamic range. For the first time, analog signal transmission using a short wavelength VCSEL is studied. We demonstrate a spurious free dynamic range suitable for personal communications systems.

The measured lasers were 20 μm x 20 μm oxide-aperture top-emitting devices fabricated at Sandia National Laboratories (Figure 12). The parasitic capacitance and resistance of the devices were measured to be 50 fF and 30 Ω , respectively. The nonlinear response of the VCSEL was measured using conventional two-tone modulation.

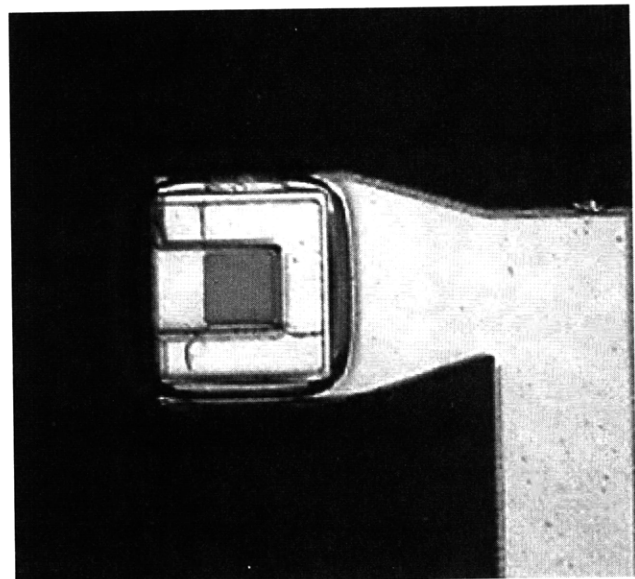


Figure 12. Oxide-apertured surface emitting laser used for signal transmission experiments.

As expected, the nonlinear response shows a power law dependence on the input power with measured exponents of 1.214, 2.201, and 3.187. The noise floor corresponds to a channel bandwidth of 1 MHz. The spurious free dynamic range (SFDR) is the ratio of the fundamental to the intermodulation product at the point where the intermodulation product crosses the noise floor. Because of the relatively low output power for the VCSEL (350 μW), the noise floor for the measured link is limited by receiver noise rather than by RIN from the laser. Figure 13 shows the dependence of the optical power and the dynamic range curve on bias current. The detuning of the gain curve from the cavity resonance due to lattice heating results in a roll-off of the optical power from the VCSEL at high current bias. This roll-off leads to a strong nonlinear response that is still observable as a plateau in the low frequency dynamic range versus current bias.

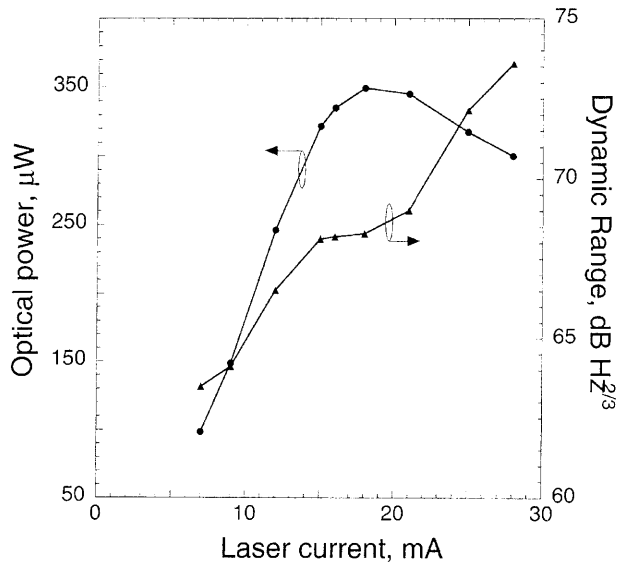


Figure 13. Spurious intermodulation free dynamic range and noise figure versus bias current for a system employing a high-speed surface emitting laser.

The maximum dynamic range was measured at 85 $\text{dB Hz}^{2/3}$ between 100 MHz and 1 GHz using a higher bandwidth detector. Although this is lower than the maximum achievable dynamic range for DFB lasers ($\text{SFDR}=125 \text{ dB Hz}^{2/3}$), these results indicate that VCSELs satisfy the dynamic range requirements for personal communication systems (PCS), which are in the range of 72-83 $\text{dB Hz}^{2/3}$. Increasing the optical power coupled into the detector and operating at higher modulation frequencies may result in

improved dynamic range for VCSEL. At higher frequencies, performance will not be influenced by thermal nonlinearities, but instead will be limited by the relatively high relaxation oscillation frequencies. In our future work, we will present the dependence of dynamic range on oxide aperture diameter illustrating the effects of spatial hole burning.

